Article

Nb₃Sn Cavities Coated by Tin Vapor Diffusion Method at Peking University

Gai Wang [1], Shengwen Quan [1,*], Lin Lin [1], Manqian Ren [1], Jiankui Hao [1], Fang Wang [1], Fei Jiao [1], Feng Zhu [1], Senlin Huang [1], Xueqing Yan [1,2] and Kun Zhu [1,2]

[1] Institute of Heavy Ion Physics & State Key Laboratory of Nuclear Physics and Technology, Peking University, Beijing 100871, China; wg6174@pku.edu.cn (G.W.); linl@pku.edu.cn (L.L.); rmq@stu.pku.edu.cn (M.R.); jkhao@pku.edu.cn (J.H.); fangwang@pku.edu.cn (F.W.); fjiao@pku.edu.cn (F.J.); zhufeng7726@pku.edu.cn (F.Z.); huangsl@pku.edu.cn (S.H.); x.yan@pku.edu.cn (X.Y.); zhukun@pku.edu.cn (K.Z.)

[2] Guangdong Institute of Laser Plasma Accelerator Technology, Guangzhou 510445, China

* Correspondence: qsw@pku.edu.cn

Abstract: Nb₃Sn-coating experiments on samples and single-cell cavities were conducted at Peking University (PKU) to understand the Nb₃Sn growth process using the vapor diffusion method. The evaporation of tin and tin chloride used in the vapor diffusion process was simulated and experimentally analyzed. The results show that the nucleation process is generally uniform, and the atomic ratios of Nb/O and Sn/O were found to be 1:2 within the 10 nm surface of the nucleated samples. Three tin sources were distributed along the cavity axis to obtain a uniform grain size on the cavity surface, and a surface tin content of 25~26% was achieved. The tin segregation effect was found in long-time coatings or coatings with insufficient tin, resulting in a low Sn% and bad cavity performance. By overcoming the tin segregation problem, a Nb₃Sn cavity with a 750 nm grain size was produced by 1200 °C coating for 80 min and 1150 °C annealing for 60 min. The acceleration gradient reached 17.3 MV/m without quenching and an obvious Q-slope at 4.2 K. The relationship between coating recipes and vertical test results is discussed and conclusive advice is provided in this paper.

Keywords: Nb₃Sn; SRF cavity; vapor diffusion method; acceleration gradient

1. Introduction

Modern particle accelerators have played a crucial role in theoretical physics, material science, radioactive medicine, and environmental science. The superconducting radio-frequency (SRF) cavity is one of the key components in a superconducting accelerator system, which is used to accelerate particles by establishing an electromagnetic field inside. For almost half a century, scientists have been dedicated to improving the performance of niobium cavities that are generally close to the theoretical physical limitation of niobium superconductor. Nb₃Sn is known to be a feasible alternative for the construction of SRF cavities with a higher quality factor and an accelerating gradient [1]. Nb₃Sn has almost double the critical temperature (18.1 K) and superheating field (420 mT) compared with niobium. The Nb₃Sn-coated cavity can contribute to building compact accelerating systems with a much lower cost than that using niobium cavities. The vapor diffusion method is proven to be the most effective method to coat cavities nowadays. In the vapor diffusion method, tin is heated into vapor to be deposited on the inside surface of niobium cavities and forming Nb₃Sn. The vapor diffusion method was first applied in the preparation of Nb₃Sn TE and TM mode cavities at Siemens AG during the 1970s [2]. A group from Wuppertal University also performed research, and they suggested the annealing step in the coating profile and proposed the necessity of a slow cooling rate for Nb₃Sn cavities [3,4].

Then, the tin vapor diffusion method was improved and developed from the Wuppertal method by Cornell University after 2009 to eliminate the Q-slope phenomenon [5,6]. Thomas Jefferson National Accelerator Facility and Fermilab also fabricated Nb_3Sn cavities with high performance via the vapor diffusion method [7,8]. Fermilab's 1.3 GHz single-cell cavity achieves a quality factor of 1×10^{10} with a nearly 24 MV/m accelerating gradient at 4.2 K, demonstrating the feasibility and prospect of Nb_3Sn-coated cavities, and representing the state of the art [8].

However, some problems regarding this issue remain to be solved. The coating profile, structure of furnaces and preprocessing greatly vary among different experiments at different institutions [9]. Additionally, the superheating field achieved is far lower than its theoretical limit. Most results of Nb_3Sn coating experiments via vapor diffusion methods exhibit a serious Q-slope phenomenon, which leads to a low accelerating gradient [3,10–15]. The grain boundary segregation effect refers to low-tin regions in the grain or the grain boundary, and film defects are confirmed to be harmful to cavity performance [16–18]. Surface roughness has also been demonstrated to influence the cavity acceleration gradient while traditional polishing methods for niobium are proven not to be so effective for Nb_3Sn [19–21].

In this work, a new coating design is proposed to apply three tin sources inside a cavity at Peking University (PKU) in order to generate uniform high-pressure tin vapor during the coating process. Samples are produced to separately study the two main processes, the nucleation stage, and the coating stage to further elucidate the differences in the deposition mechanism between a single-tin-source design and a three-tin-source design. Nb_3Sn coating experiments are also carried out on 1.3 GHz single-cell Tesla-type cavities using different recipes, and a detailed analysis is presented in this paper.

2. Experimental Descriptions

2.1. Coating Procedure at PKU

The schematic diagram of the furnace for Nb_3Sn coating at PKU is shown in Figure 1. The furnace consists of two vacuum systems. The inside chamber is made of pure niobium, and the initial vacuum can reach 10^{-5} Pa after 48 h of 200 °C degassing. The furnace has a total of six C-type thermocouples to measure the temperature of the outer wall of the inner chamber and one thermocouple to measure the temperature of the outer wall of the evaporating boat area. The temperature control system was experimentally calibrated twice to eliminate the error between temperatures inside and outside the wall of the chamber. This furnace was located in a relatively clean room.

In other typical coating devices for single-cell cavities, the tin source is put at the bottom of the cavity and tin vapor rises to the inside of the cavity [3,6,8–10,13–15]. We found that the location of the tin source influences the distribution of the tin vapor pressure, which is one of the key parameters during Nb_3Sn growth. In our previous single-tin-source experiments, the grain sizes and morphology varied at the top and bottom of the cavity. Therefore, a new tin source arrangement was proposed: three tin sources were put inside the cavity, along the center cavity axis. The tin was stored in small tungsten evaporation boats supported by a 2.5 mm diameter niobium wire, as shown in Figure 2. The distances of the sources from the cavity top were 100 mm, 230 mm, and 420 mm. Detailed comparisons are described in Section 3.3.

The upper beampipe of the niobium cavity was covered by niobium foil. The nucleation agent $SnCl_2$ was stored in a tungsten crucible with an independent heater at the bottom of the chamber. Several small niobium strips or sheets were suspended on the central axis of the cavity as witness samples in every coating experiment. The samples were as small as possible considering that big samples may disturb the tin vapor flow resulting in nonuniform Nb_3Sn coatings. Each cavity was buffered chemical polished (BCP) and high-pressure water rinsed (HPR) before loading into the furnace.
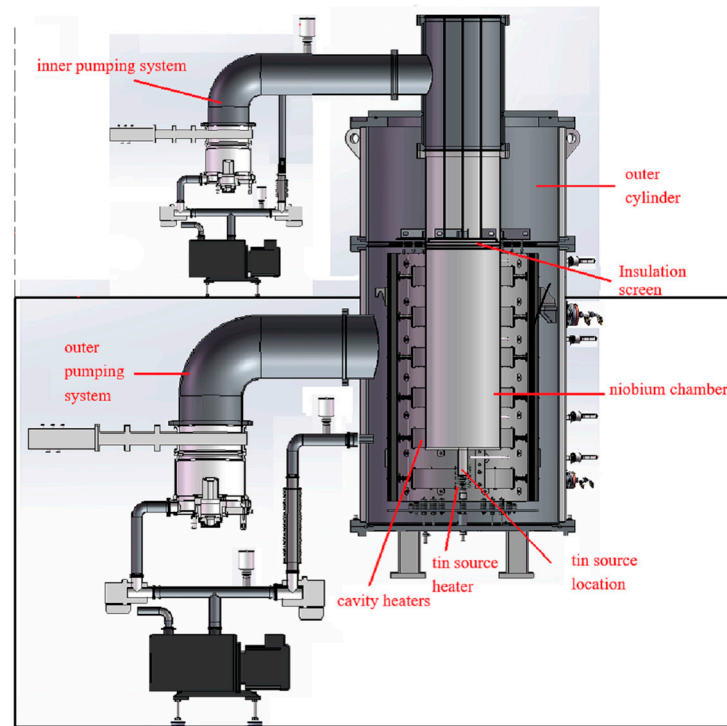
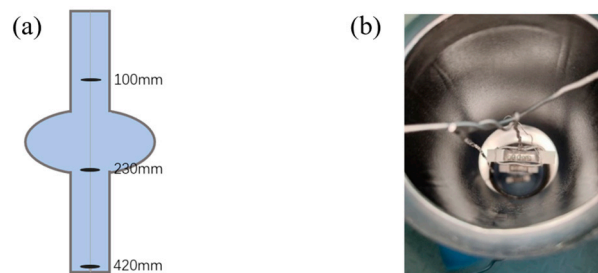**Figure 1.** Scheme diagram of the furnace for Nb$_3$Sn coating at PKU.

Figure 2. (**a**) Schematic of three-tin-source coating design; the tin sources are hung inside the cavity, and the distances of the sources from the cavity top are annotated; (**b**) photo of cavity interior.

The typical temperature profile and the vacuum measurements are shown in Figure 3. In the nucleation stage, the SnCl$_2$ crucible was heated rapidly to 800 °C and kept for 30 min. The vacuum valve of the molecular pump was closed, and during the whole coating process, the vacuum was measured by a film gauge with a measurement range of 0.01–10 Pa. During this procedure, SnCl$_2$ was fully evaporated, and its pressure reached 1 Pa. Then, the SnCl$_2$ crucible cooled down to 500 °C or 650 °C for 4.5 h. The cavity was mounted on a niobium tube to maintain distance from the high-temperature region so that the two temperature regions did not interfere with each other. Then, the cavity temperature was ramped up to 1150–1200 °C and maintained for 2~5 h. Lastly, the system cooled down naturally.

2.2. Nucleation Experiments

The BCP-ed samples received the nucleation process with different parameters and were taken to material tests. Every nucleation experiment used a single-cell 1.3 GHz cavity to offer a similar evaporation environment, and after the experiment, the cavity was BCP-ed lightly to remove surface contaminations created by nucleation.
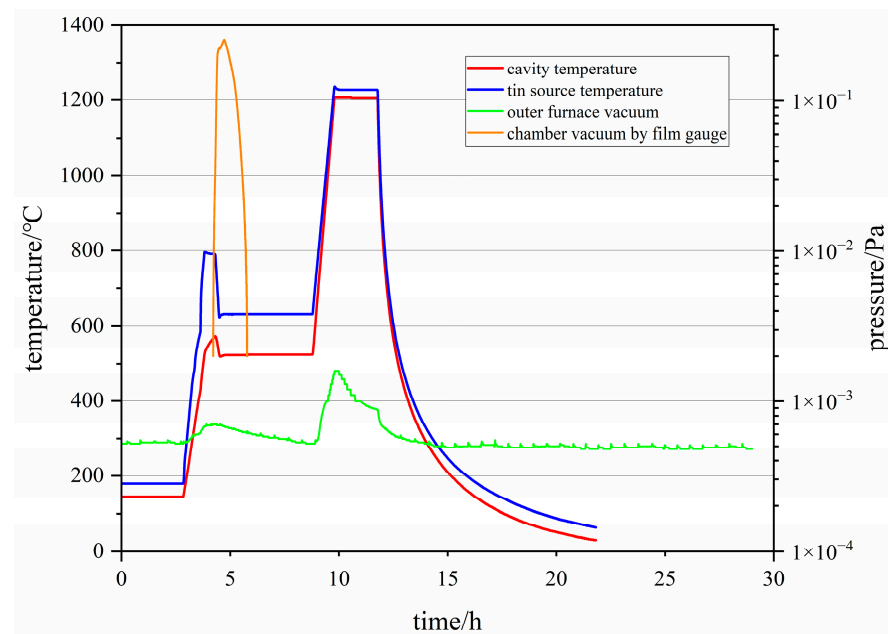
Figure 3. A typical temperature profile for Nb$_3$Sn cavity at PKU, the degassing stage is not shown.

The nucleation parameters of five nucleation experiments are shown in Table 1. The first two nucleation experiments used a perforated cavity, which means tin chloride would diffuse through the holes and run out of the cavity. The last three nucleation experiments used a whole cavity with niobium foil covering its top beam port. Additionally, SnCl$_2$ and Sn were put in the same tungsten boat at the bottom of the chamber in the 1st and 2nd nucleation experiments while three tin sources were used inside the cavity in the 3rd–5th experiments. The nucleation temperature was set at 500 °C in these experiments.

Table 1. Nucleation experiments parameters.

Number	Assembly	Tin Source	Amount of SnCl$_2$/Sn	Nucleation Time
1	cavity with holes	single	3 g/0 g	5 h
2	cavity with holes	single	3 g/1.5 g	5 h
3	cavity	three	3 g/2.4 g	5 h
4	cavity	three	6 g/2.4 g	5 h
5	cavity	three	3 g/2.4 g	8 h

2.3. Coating Stage Study

In this study, we carried out three-tin-source coating experiments on cavities and samples with different coating times, coating temperatures and amounts of tin. The temperature ramping rate was 10 °C/min. The nucleation profiles of these experiments were the same as those of the 3rd nucleation experiment in Section 2.2 except for the 23rd coating, which used a nucleation time of 8 h. After coating, the cavities were vertically tested at 4.2 K, and witness samples were ultrasonically cleaned and brought to analysis. Detailed experimental variations are shown in Table 2.

Table 2. Coating stage study experimental parameters.

Number of Experiments	Number of Cavities	Tin Weights/g	Tin Chloride Weights/g	Coating Temperature/°C	Coating Time/min	Annealing Temperature/°C	Annealing Time/min
12	NS01	0.3 + 0.4 + 0.5	3	1150	300	-	-
13	NS04	0.6 + 0.8 + 1.0	3	1150	300	-	-
14	NS01	0.6 + 0.8 + 1.0	3	1200	300	-	-
15	NS03	0.6 + 0.8 + 1.0	3	1200	150	-	-
16	NS02	0.6 + 0.8 + 1.0	3	1200	120	-	-
17	NS06	0.6 + 0.8 + 1.2	3	1150	120	-	-
19	NS04	0.6 + 0.8 + 1.0	3	1150	90	1100	60
22	NS01	0.6 + 0.8 + 1.0	3	1200	90	1100	60
23	NS02	0.6 + 0.8 + 1.0	3	1200	90	1100	60

3. Results Analysis

3.1. Simulation Analysis of the Vapor Pressure in the Nucleation Stage and Coating Stage

In order to find out the reason that causes the variations in grain size along cavity axes in previous experiments with a single tin source, tin and tin chloride evaporation was analyzed theoretically.

First of all, in the nucleation stage, the vapor pressure of tin was quite small, about 10^{-6} torr at 800 °C, and tin chloride was dominant. The saturated vapor pressure of tin chloride was larger than several kPa·s [22]. Then, the evaporation rate of the tin chloride could be derived using the Langmuir Formula (1) and the Knudsen number K_n could be calculated by Formulas (2) and (3), where $\frac{dM}{dt}$ is the evaporation rate of the tin chloride, A is the evaporation area, P is the vapor pressure, m is the atom mass, k_B is the Boltzmann constant, T is the vapor temperature, λ is the mean free path, d is the diameter of the atom and D is the characteristic length of 300 mm [23,24]. The results are shown in Figure 4a. It can be seen that $K_n < 0.01$, which means viscous flow. The evaporation rate is above 300 g/s at 800 °C, which means 3 g tin chloride would turn to gas in the front stage of nucleation. This derivation assumes the tin chloride vapor is the ideal gas and evaporates at saturated pressure, while actual evaporation can be faster due to a low level of the initial vacuum. Then, the pressure of the tin chloride vapor is supposed to be distributed by gravity after diffusion, as shown in Figure 4b. The pressure gradient between the top and bottom of the cavity is small, allowing us to conclude that the nucleation agent is evenly distributed inside the cavity.

$$\frac{dM}{dt} = AP\sqrt{\frac{m}{2\pi k_B T}} \tag{1}$$

$$\lambda = \frac{k_B T}{\sqrt{2}\pi d^2 P} \tag{2}$$
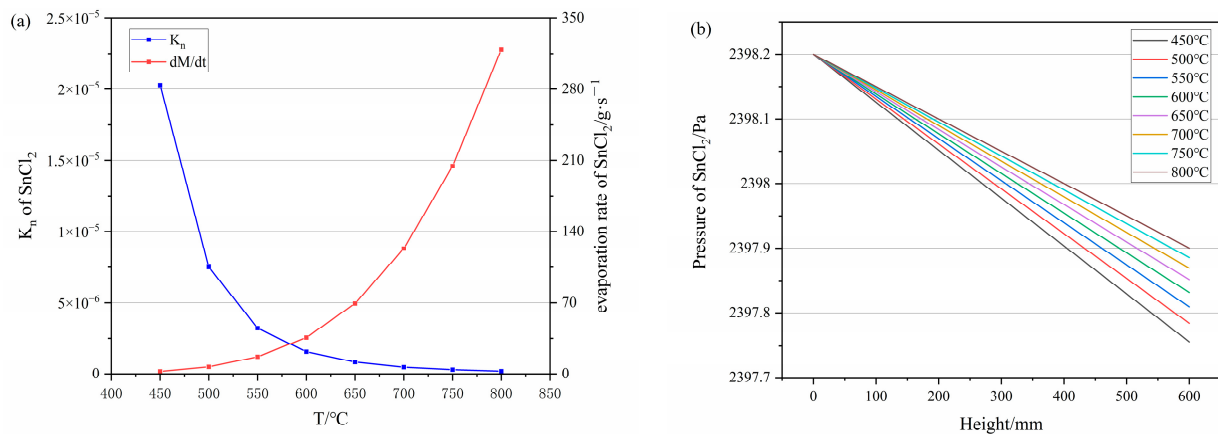
$$K_n = \frac{\lambda}{D} \tag{3}$$

Figure 4. Calculations for tin chloride: (**a**) Knudsen number and evaporation rate at 450–800 °C of tin chloride, calculated from Formulas (1)–(3); (**b**) presents the vapor pressure at different temperatures and heights, showing that the vapor pressure of tin chloride is uniform inside the cavity.

The vapor pressure of tin is negligibly low in the nucleation stage, but tin is the main part of the gas in the coating stage while tin chloride vanished. R. Ridgway simulated the tin particle flux on the cavity wall at a temperature of 1400 °C using the free molecular flow module and revealed the importance of the high temperature of the tin source [25]. We simulated the tin evaporation at 1100–1300 °C using the slip flow module in COMSOL Multiphysics. The tin vapor follows a transitional flow, corresponding to the Knudsen number presented in Figure 5a. The evaporation rate used is calculated by Formula (1), shown in Figure 5b. In this model, the cavity upper port is open and only one tin source

is used. It is difficult to measure the absorption rate of tin at the cavity wall; we only consider that little tin is absorbed into the walls and most tin vapor flows out through the top end, which may happen in the initial state of the coating stage or after a long time of coating. From the simulation results in Figure 6, pressure at the bottom is nearly 10 Pa while pressure in the upper region is only 2 Pa, which could result in a smaller grain on the upper cavity wall.
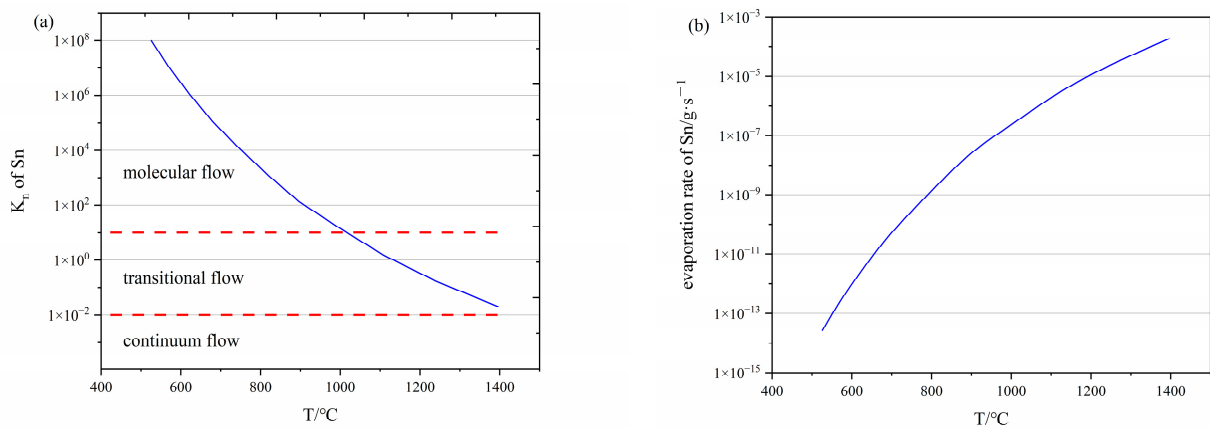
Figure 5. Calculations for tin: (**a**) Knudsen number and (**b**) evaporation rate at 500–1400 °C; the tin vapor follows transitional flow at 1100–1300 °C.
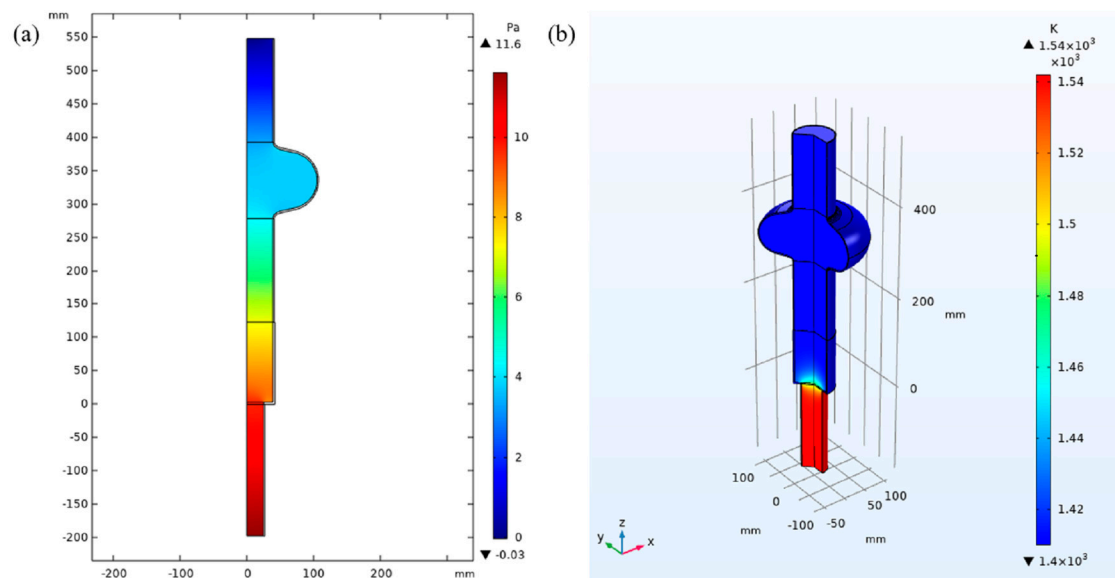
Figure 6. Pressure and temperature of the tin vapor were simulated using slip flow module in COMSOL; (**a**) presents the vapor pressure, which is nonuniform in the vertical direction; (**b**) shows the temperature of tin vapor.

3.2. Roles of Nucleation in Vapor Diffusion Method

The single tin source located at the bottom of the chamber seems to generate a non-uniform tin vapor inside the cavity in the coating stage, which may result in a height-dependent Nb_3Sn growth rate in our previous experiments due to the last section's simulation. In this section, the nucleation stage is discussed in detail from the experimental perspective, and the coating stage is discussed in Section 3.3.

Nucleation experiments with different nucleation times and amounts of nucleation agents were studied via SEM. First of all, obvious nucleation sites appear on the sample surface in nucleation experiments with tin and tin chloride, but no nucleation site was

found on samples from the nucleation with only tin chloride in the 1st experiment. It is supposed that the tin may participate in the nucleation process. Figure 7 shows the surface nucleation sites obtained by SEM. Triangular, circular, and polygonal nucleation sites can be found in the nucleated samples with a single tin source. The triangular-shaped nucleation sites appeared at the upper part of the cavity, exhibiting a smaller coverage rate of tin particles compared to the other two. The nucleation sites were only found to be circular in three-tin-source nucleation.
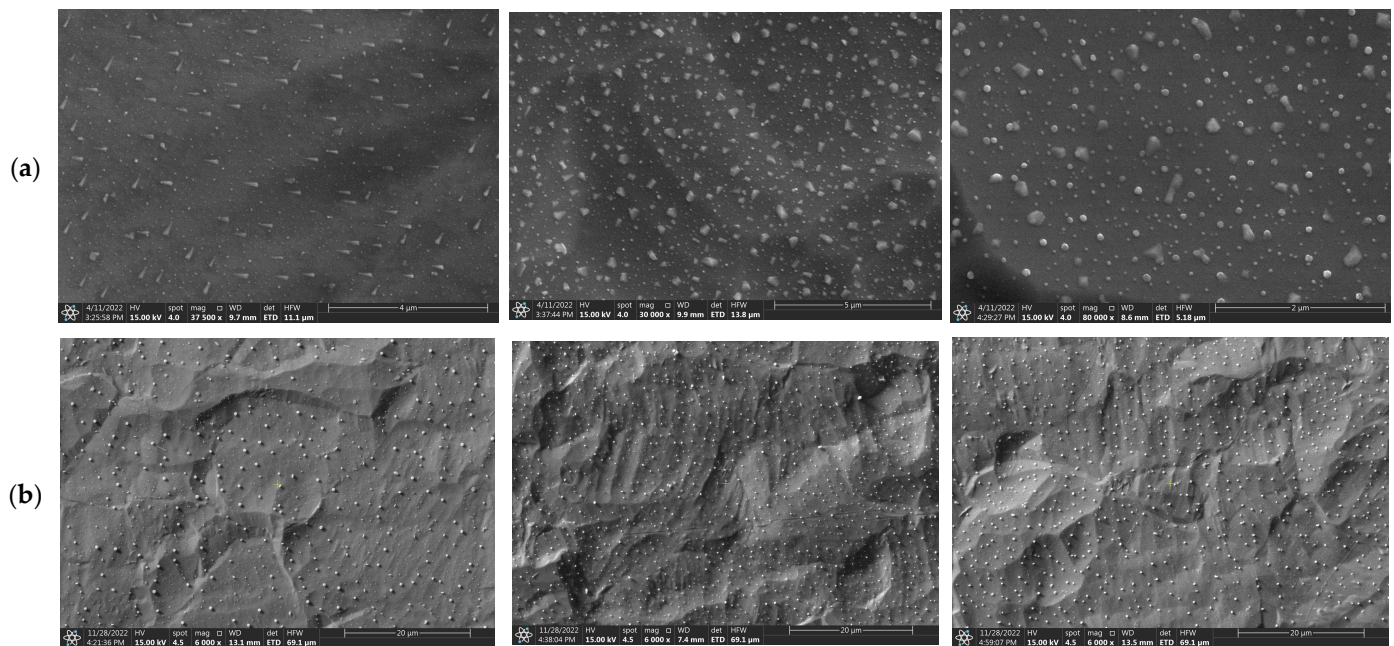

Figure 7. (**a**) SEM pictures of triangular, polygonal, and circular nucleation sites from single-tin-source nucleation, the magnification is about 30,000; (**b**) SEM pictures of circular nucleation sites from three-tin-source nucleation, the magnification is about 6000.

ImageJ software is applied to analyze these nucleated particles. ImageJ has powerful capabilities in cytometric analysis, which can treat these nucleated sites as well. Figure 8 shows SEM pictures before and after treated by ImageJ. The coverage rate of the tin particles obtained by this method is affected by the resolution of the SEM; therefore, the results are compared at the same magnification of $3000\times$. The coverage rates of tin particles have slight differences, shown in Figure 9. The single-tin-source results have much a smaller nucleation site area and larger coverage rates compared with three-tin-source nucleation, probably because the tin source is pre-heated to 800 °C together with tin chloride in the single-tin-source experiment but the three tin sources are not pre-heated.

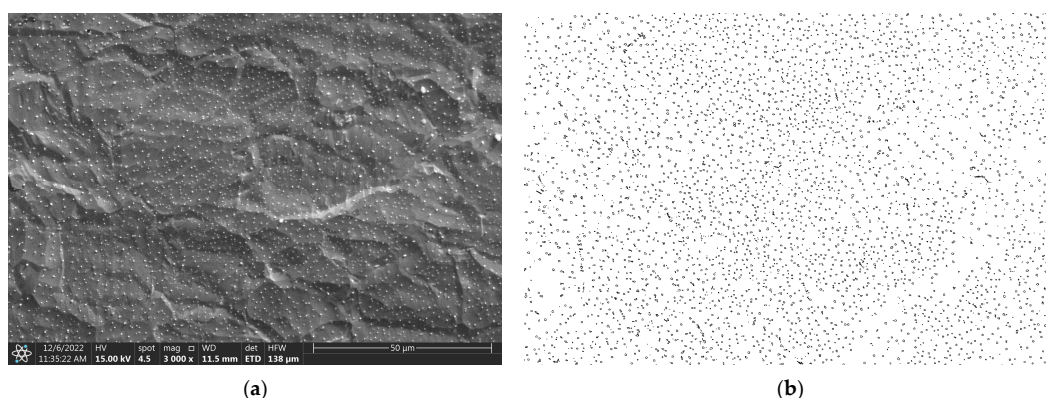**Figure 8.** The nucleation sites extracted (**b**) from the preliminary SEM picture (**a**) by ImageJ.
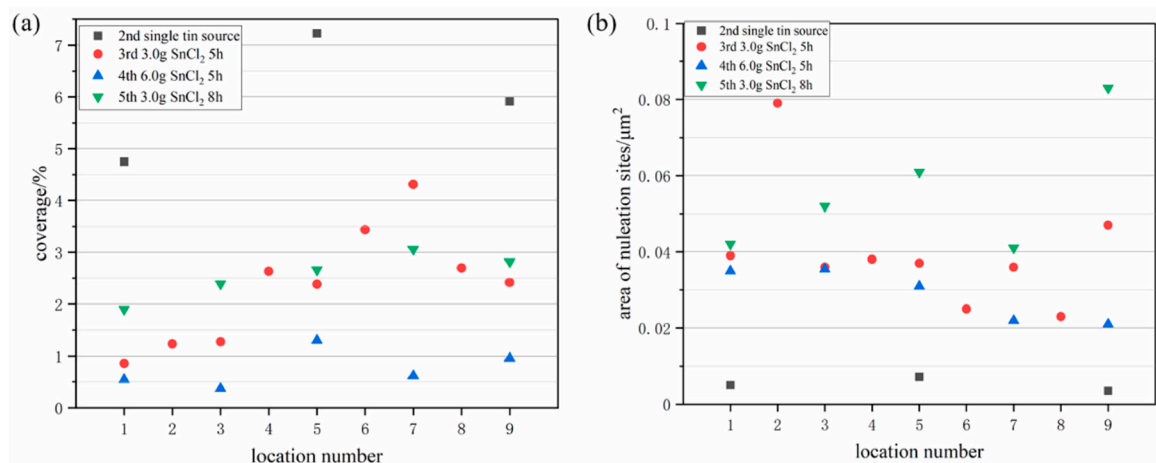
Figure 9. (**a**) Tin particle coverage rates and (**b**) area of nucleation sites from 2nd–5th nucleation experiments; the data are calculated from ImageJ-treated SEM figures.

Comparing the results of 3.0 g and 6.0 g $SnCl_2$ for 5 h nucleation, it is found that using more tin chloride makes the tin particle smaller and decreases the coverage rate. Using a longer nucleation time will slightly increase the nucleation area coverage and average area, which can be discovered from 3.0 g $SnCl_2$ nucleation for 5 h and 8 h. These phenomena are similar to reports by U. Pudasaini [26].

For a better understanding, these nucleated samples were tested via XPS using Argon ion sputtering. It was found that carbon and oxygen contaminations existed, shown in the XPS spectrum in Figure 10. The XPS typically had a detection range of 10 nanometers and the energy spectrum of each sample was measured before and after 15 nm sputtering in order to measure the relative quantity within 0–10 nm and 15–25 nm. The atomic ratio result of the single-tin-source nucleation is displayed in Table 3. To highlight the depth distribution of tin, the relative proportions of tin to niobium were calculated and Sn/(Nb + Sn)% values are shown in Figure 11. The single-tin-source Sn/(Nb + Sn)% value is higher than the other three, probably because the tin was stored in the bottom boat and an amount of tin evaporated during the high-temperature pre-heating period, which proves again that the tin vapor participates in the nucleation sites forming. It can be seen that the Sn/(Nb + Sn)% value is larger with more $SnCl_2$ applied from the results of 3.0 g and 6.0 g $SnCl_2$ nucleation. There is no difference between the 3rd and 5th Sn/(Nb + Sn)% values which correspond to different nucleation times. There is no significant distinction of Sn/(Nb + Sn)% values among the upside, middle, and downside samples of 3.0 g $SnCl_2$ 5 h and 8 h nucleation, which means that the nucleation is generally uniform along the cavity axis.

Table 3. XPS elements analysis data from 2nd nucleation experiment (3 g $SnCl_2$, 1.5 g Sn, 5 h, single tin source).

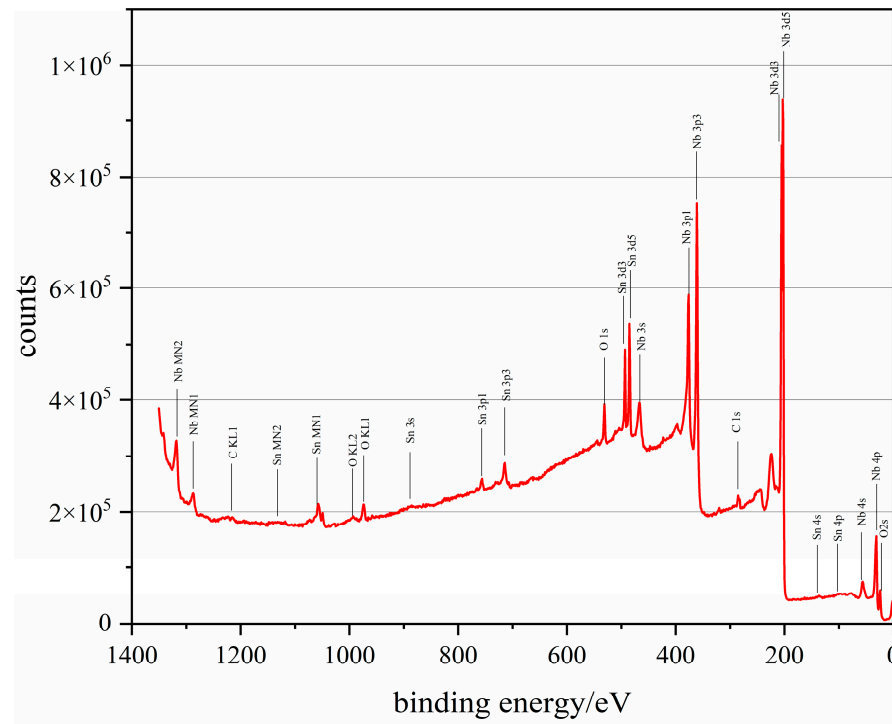| Location		C%	O%	Nb%	Sn%	$\frac{Sn}{Sn+Nb}$%
up	0 nm	51.85	32.22	8.32	7.61	48
	15 nm	27.74	19.32	44.93	8.01	15
middle	0 nm	55.35	30.08	8.19	6.38	44
	10 nm	23.91	21.22	49.10	5.77	11
bottom	0 nm	44.04	37.40	10.50	8.06	43
	15 nm	18.33	21.78	54.69	5.21	9

Figure 10. XPS spectrum of a nucleated sample after sputtering. C and O are found in the spectrum; data are from 2nd nucleation experiment (3 g SnCl$_2$, 1.5 g Sn, 5 h, single tin source).
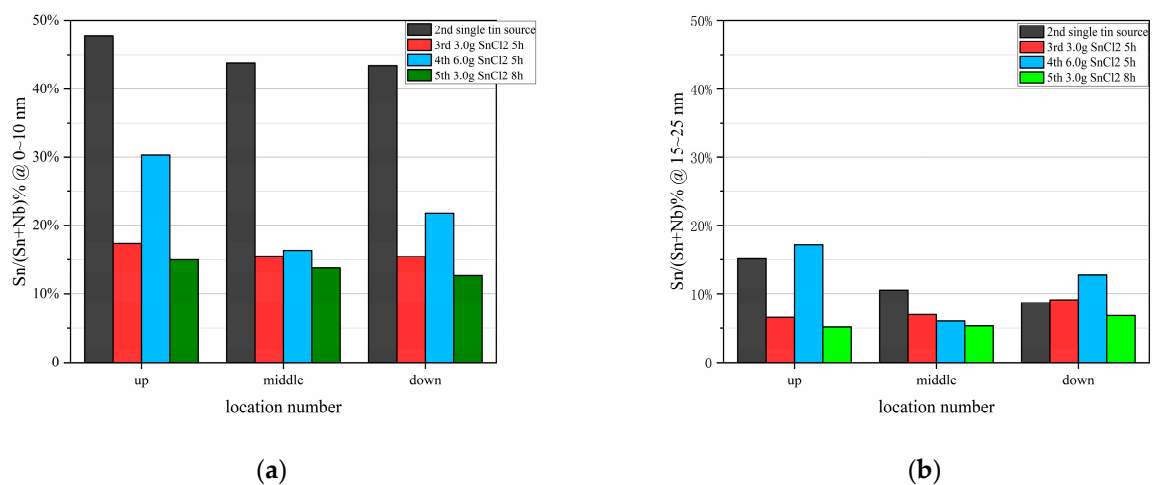

(**a**)　　　　　　　　　　　　　　　　　　　(**b**)

Figure 11. Sn/(Sn + Nb)% of samples within 0–10 nm (**a**) and 15–25 nm (**b**) from the nucleation experiments, measured via XPS.

The detected carbon may have come from adsorbed carbon in the air or inside the furnace, and the oxygen is proposed to have originated from the niobium substrate. The contents of elemental carbon and oxygen decrease faster with depth than tin, representing that they mainly exist at the surface.

It is worth mentioning that in every nucleation experiment, the contents of oxygen, niobium, and tin in the 1–10 nm range satisfy the linear relationship, O% = 2 × Nb% + 2 × Sn%, indicating that tin and niobium may exist as NbO$_2$ and SnO$_2$ at the 1–10 nm surface. Figure 12 shows the linear fit results between O%/Sn% and Nb%/Sn%. Oxygen from the niobium substrate may help the surface capture tin atoms from the vapor, a possible

reaction is given in Formula (4), which needs to be further verified. There is no linear relationship between the contents of Nb, Sn, and C.
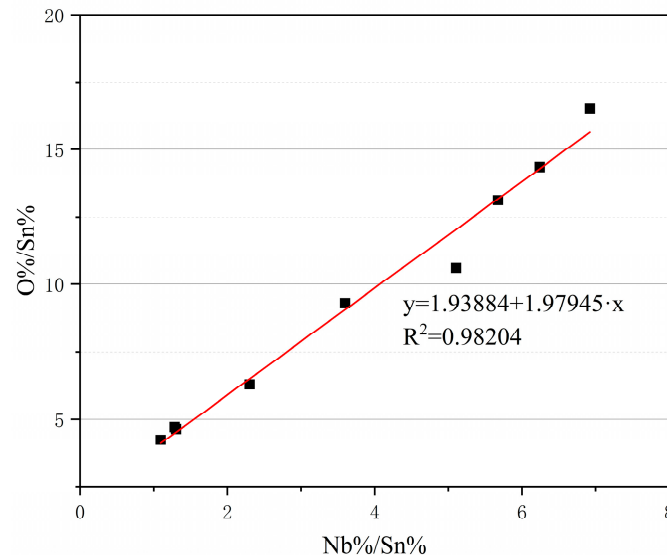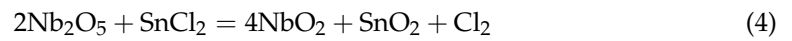
$$2Nb_2O_5 + SnCl_2 = 4NbO_2 + SnO_2 + Cl_2 \qquad (4)$$

Figure 12. Linear fit result of the Nb, Sn, and O contents; y and x present the ratios of O/Sn and Nb/Sn, respectively, both of which are close to 2.

These nucleated samples were sent to the furnace and only dealt with the coating stage to find any difference in the final Nb_3Sn films. The samples were analyzed via SEM and EDS. Insignificant differences were found in the grain topography and surface tin content.

3.3. Differences between Single-Tin-Source and Three-Tin-Source Coatings

In the early coating experiments with one tin source and ~200 °C temperature gradient between the tin source and the cavity, witness samples at three positions along the cavity axis were found with disparate features. SEM photos from these experiments are presented in Figure 13. It can be found that the samples hung at the bottom of the cavity have hollow grains and the grains of the upside sample are smaller than the downside.

We designed a new coating setup with three different amounts of tin sources inside the cavity to decrease the distance between the tin source and the cavity surface. This kind of setup has two advantages:

- Making the tin vapor pressure more uniform in the vertical direction;
- Avoiding the risk of excessive liquid tin condensation because the tin sources always have a lower temperature than the cavity.

The curves of average grain size (AGS) versus height of single-tin-source coatings and three-tin-source coatings are displayed in Figure 14. The AGS was calculated by the MATLAB script, based on the line intersection method [27]. Figure 14 shows that the uniformity of the grain size is improved by decreasing diffusion distance and dispersing evaporation sources. In brief, the coating stage is the main process that determines the grain uniformity at different heights, and the three-tin-source design is proven to generate tin vapor with uniform pressure according to these experimental data and analyses in Sections 3.1 and 3.2.
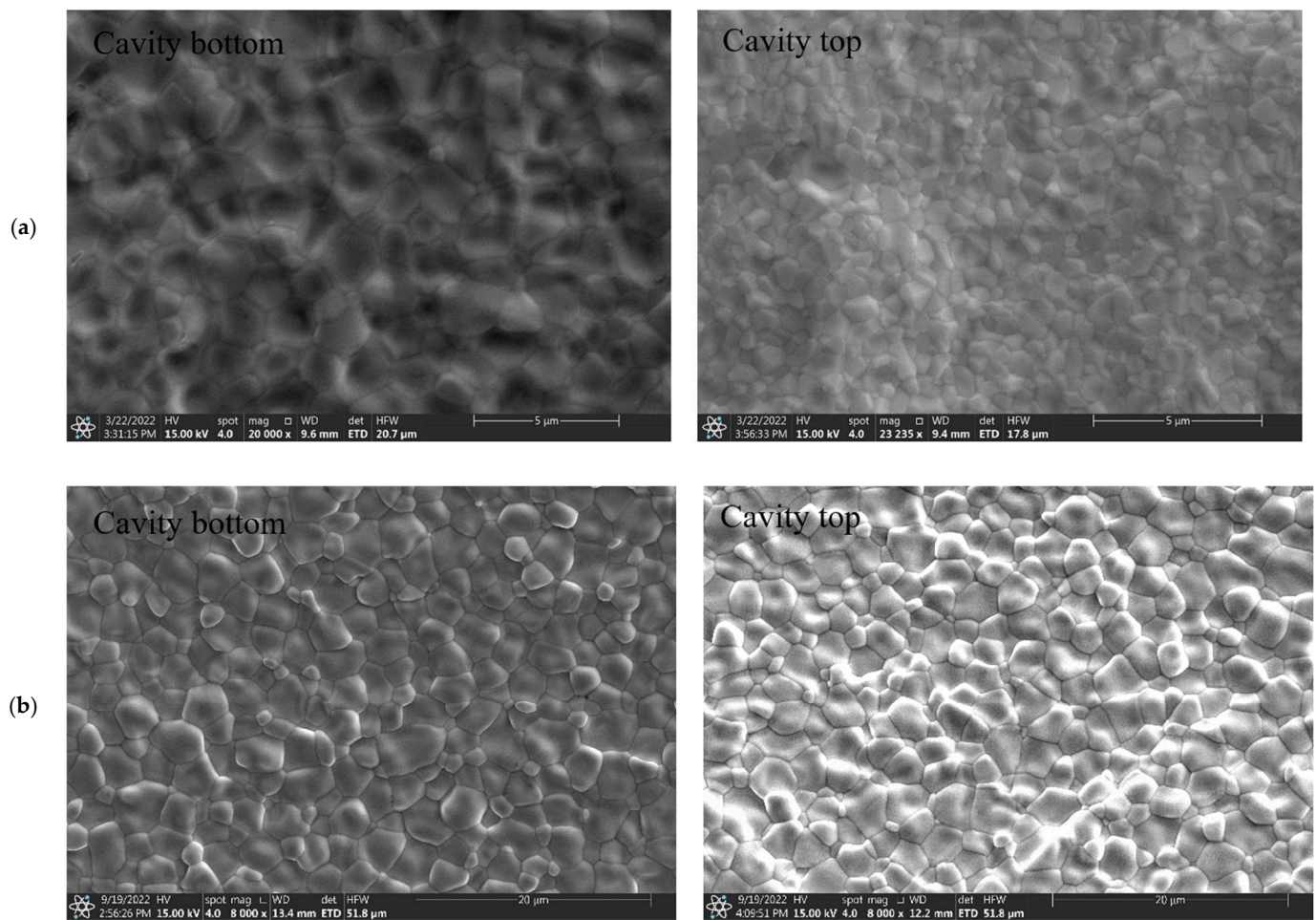
Figure 13. SEM pictures of samples at the top and bottom of the cavity; (**a**) is from a single tin source and (**b**) is from three tin source coatings.
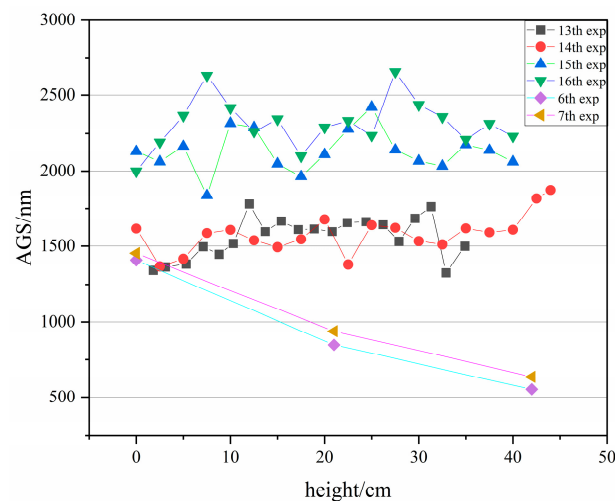

Figure 14. The curve of AGS versus height from single tin source (6th and 7th) and three tin source (13th–16th) coatings.

3.4. Tin Segregation Effect and Principles of Coating Stage

Discussions in this section are focused on how different coating stage parameters affect the coatings. Samples from the 12th to the 19th experiments were SEM/EDS-tested to measure the surface Sn% and the grain sizes. The tin segregation effect was observed on

the 12th, 13th, and 14th witness samples. The tin content of the surface is determined by the reaction rate and the evaporation rate of the surface, which can be controlled by coating temperature and time for a certain amount of tin usage. As the evaporation continues, the pressure decreases and the reaction rate decreases to less than the evaporation rate in the surface, and the tin begins to segregate from the Nb_3Sn surface.

Thus, an insufficient tin supply or too long a coating time will cause a tin segregation effect. In the 12th experiment, Nb_3Sn grains were incomplete, and the grain boundaries were inconspicuous, due to only 1.2 g of tin being utilized.

In the 14th–16th coatings, the tin sources were consumed completely, and the coating temperature was the same at 1200 °C, but the coating times were 300 min, 150 min and 120 min, respectively. The samples were TEM/EDS-tested to obtain the Nb_3Sn thickness and cross-sectional Sn%. From the test results, surface Sn%, cross-sectional Sn%, grain size and thickness all decrease with the coating time, as shown in Figure 15. The sample of 300 min coating gives a morphology feature of holes inside the grain, while the samples of 150 min and 120 min coating have no tin segregation effect and show complete grains.
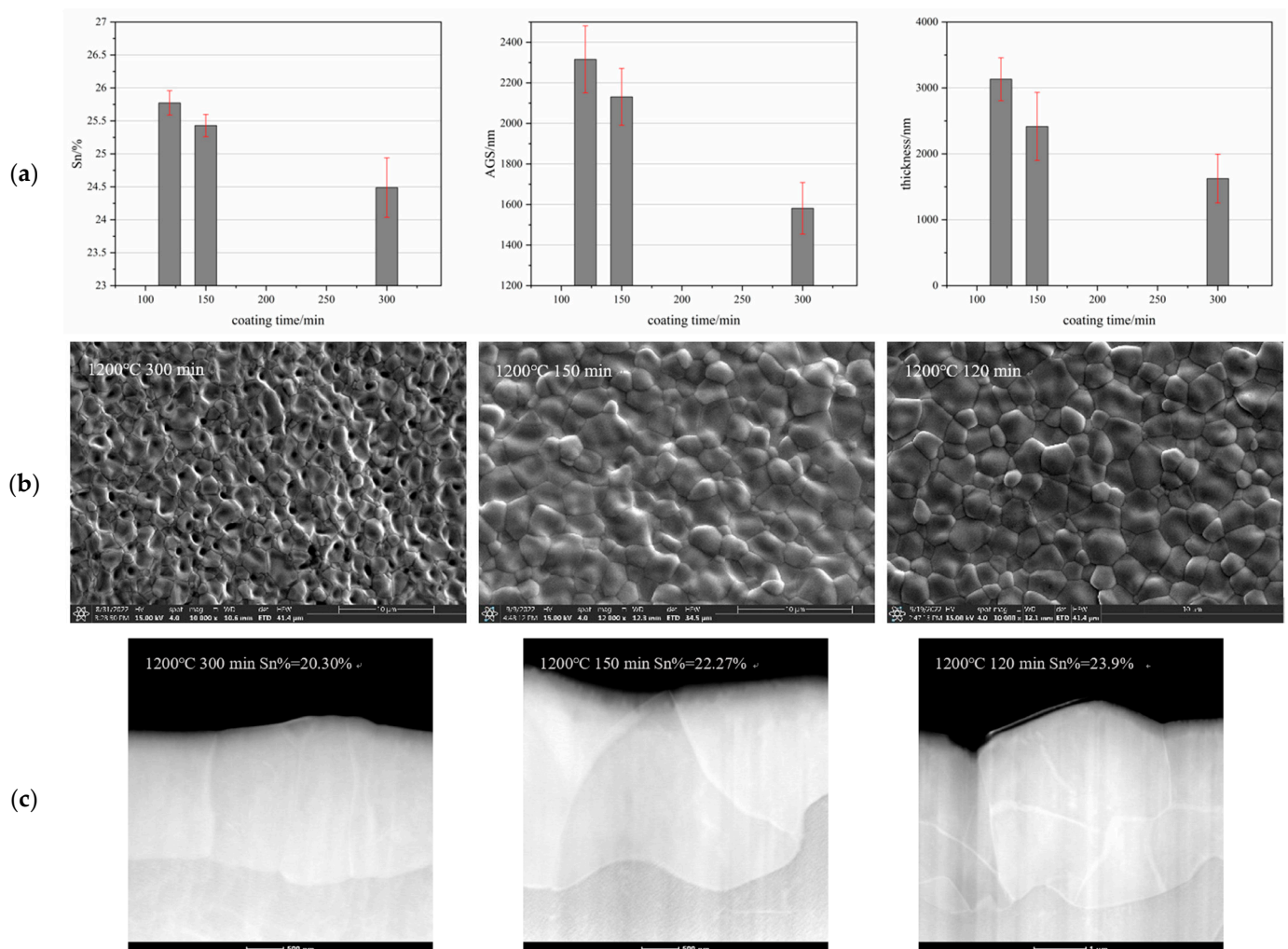

Figure 15. Comparisons of 1200 °C 300 min, 1200 °C 150 min, and 1200 °C 120 min coatings: (**a**) surface Sn%, AGS, and average depth of the Nb_3Sn films; (**b**) SEM photographs of Nb_3Sn grains with and without tin segregation effect; (**c**) TEM photographs of Nb_3Sn films; cross-sectional Sn% is annotated.

Comparing 1150 °C 300 min and 1200 °C 300 min samples with tin segregation, the tin segregation effect became worse with increases in temperature. When the coating temperature changed from 1150 °C to 1200 °C, the film thickness decreased from 1796.6

$\pm$ 0.24 nm to 1624.1 $\pm$ 0.37 nm, and the cross-sectional Sn% also decreased from 24.4% to 20.3%.

The normal Nb_3Sn coatings in the 16th, 17th, 19th, 22nd, and 23rd experiments have similar topography; the Sn% and AGS comparisons are given in Table 4. It can be found that the growth of Nb_3Sn at 1200 °C is faster than that of 1150 °C compared with the 16th and 17th coatings. The tin contents are generally larger than 25%, even achieving 26% in our coatings, which exceeds the levels of 24~25% reported by other institutions [7,13–16]. Subsequently, we attempted to add an annealing stage at 1100 °C and reduce the coating time to 80 min in 19th, 22nd, and 23rd experiments in order to reduce the temperature and vapor pressure of the tin vapor and adjust the tin content in the film to 25%. It can be seen that annealing can lightly reduce the grain size and help lower the surface Sn%.

Table 4. Results and parameters of 16th, 17th, 19th, 22nd, and 23rd experiments.

Experiment	Sn% by SEM/EDS	AGS/nm	Coating Temperature/°C	Coating Time/min	Annealing Temperature/°C	Annealing Time/min
16	25.8	2316	1200	120		
17	26.1	1748	1150	120		
19	23.7	740	1150	80	1100	60
22	25.4	909	1200	80	1100	60
23	25.4	854	1200	80	1100	60

3.5. Cavity Vertical Tests

All the coated Nb_3Sn cavities were vertically tested at 4.2 K temperature at PKU. The Nb_3Sn cavities received the standard HPR procedure before the vertical test. The ambient magnetic field was less than 2 mg. A slow cooling rate of 5–10 min/K was applied from 25 K to 15 K to minimize additional flux penetration originated by the Seebeck effect. The transition temperatures of cavities without Sn segregation were near 18 K, measured during the vertical test. The results of the cavity vertical tests are shown in Figures 16 and 17. Obviously, the 15th–19th cavities without the tin segregation effect have a better performance than the 12th and 14th cavities whose grains are incomplete and have holes. The Q of the NS02 cavity from the 16th experiment reached 4.82×10^9 @ 0.7 MV/m but decreased with E_{acc} rapidly. The 15th, 16th, and 17th cavities all had a strong Q-slope, and the maximum E_{acc} is 10.5 MV/m due to the power limit.
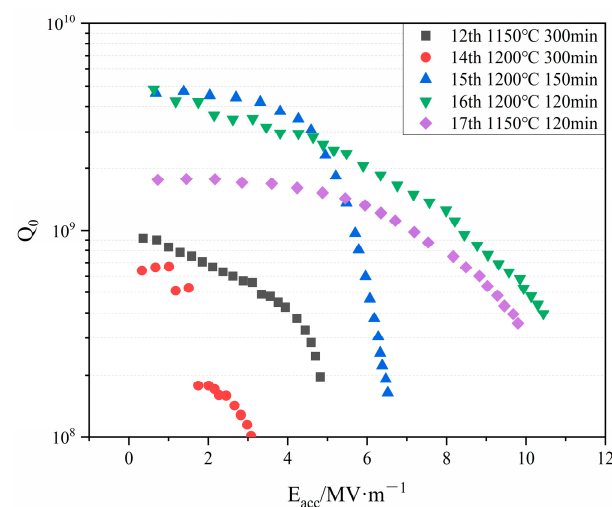

Figure 16. The 4.2 K vertical test results of the 12th–17th coated cavities without the annealing stage noted that the 12th and 14th cavities have a bad tin segregation effect; the maximum Q (from the 16th experiment) reaches 4.82×10^9 @ 0.7 MV/m.
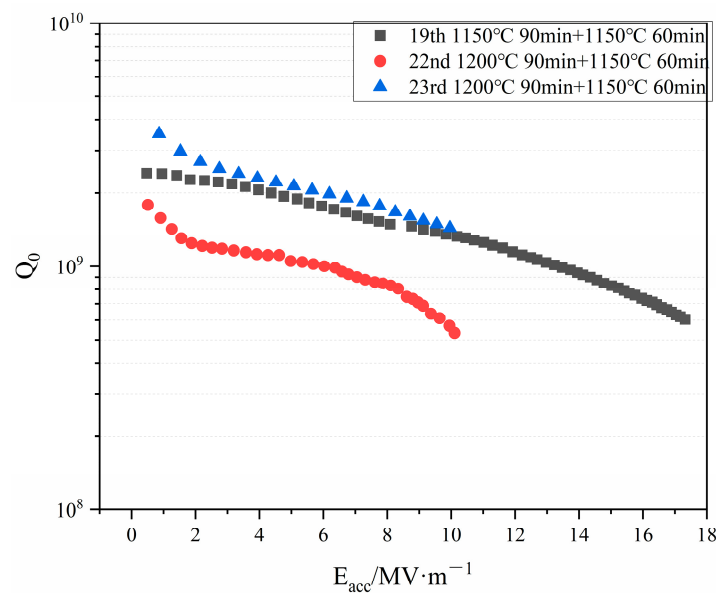
Figure 17. The 4.2 K vertical test results of the 19th, 22nd, and 23rd coated cavities with the annealing stage; the maximum gradient (from the 19th experiment) reaches 17.3 MV/m.

The 19th, 22nd, and 23rd cavities coated with an annealing stage have relatively flat Q-E curves. The 19th NS04 cavity reaches a maximum gradient of 17.3 MV/m limited by power, and the 23rd NS02 cavity has a similar performance. We believe that two types of curves from cavities with and without annealing have different patterns because the tin contents vary. J. Lee's work proposed that grain boundary tin segregation can cause the Q value to degrade with the accelerating field [16]. The annealing stage may improve the situation of excess tin inside the grain or grain boundary after the coating stage, corresponding to the EDS results from the witness samples. Excess tin atoms inside the grain lattice are dangerous for cavity superconductivity; once the Sn atoms form normal conducting lattices larger than the coherence length, the cavity would quench.

Here, we give three possible reasons for these Q values being lower than 1×10^{10}.

- Carbon contamination was found on the surface of samples from most coating experiments;
- Recrystallization of niobium cavities due to long time baking, which might cause the nucleation non-uniformity among Nb grains with different orientations, forming patchy regions and increasing the surface roughness;
- Excess tin in the grain would help trap more flux and create extra surface resistance.

4. Discussions

4.1. Summary of Present Work

The nucleation stage and coating stage of the tin vapor diffusion process are studied separately on witness samples and cavities. Here is a summary of the main results.

- The location of the tin source influences the vapor pressure distribution and grain growth. A three-tin-source setup will make the coating more uniform along the cavity axis and prevent liquid tin condensation on the cavity. Moreover, the surface Sn% can reach beyond 25% through this setup, compared with a second heater set proposed by Cornell University [28];
- The topography of the nucleation site is slightly affected by the nucleation time or the amount of nucleation agent $SnCl_2$, but the final Nb_3Sn films show no obvious differences. Tin is found to probably form SnO_2 within 10 nm of the surface;

- The tin segregation effect has been discovered in coatings of long coating times and insufficient tin. Tin would segregate from the Nb_3Sn grains, reducing the grain size and surface Sn%, creating holes in the surface center of the grain. The tin segregation effect is harmful to cavity performance;
- Annealing at 1100 °C has been experimentally proven to decrease the Q degradation with the acceleration gradient.

4.2. Limitations of Present Work and Future Plans

First of all, our experimental analysis is based on the witness samples hung along the axis of the cavity which could not represent the actual situation of Nb_3Sn coating at the cavity equator.

The recent Q of Nb_3Sn-coated cavities at 4.2 K is generally lower than 1.0×10^{10}, which needs to be increased by controlling the tin content in the grain and the boundary and improving the topography of the Nb_3Sn film. The parameters of the nucleation stage and the annealing stage should be carefully designed after comparison experiments, while the tin distribution in the grain should be measured using high-resolution methods. Ellipsometry would be used to measure the thickness for comparison with existing data [29]. Furthermore, the chamber environment should be fully checked and cleaned to eliminate any possible contamination sources in the future.

The actual influence of recrystallization is not clear yet. Research on recrystallization by coating large-grain niobium samples with different grain orientations will be carried out.

5. Conclusions

We have studied the fabrication of a Nb_3Sn cavity via the tin vapor diffusion method, using witness samples and a 1.3 GHz Tesla-type single-cell cavity. The nucleation and coating processes are analyzed theoretically and experimentally. The results demonstrate that the nucleation is uniform along the cavity axis, and normal Nb_3Sn with an evenly distributed grain size is obtained using the three-tin-source coating design and choosing a suitable coating time and temperature. The tin segregation effect reduces the surface Sn% and creates defects on the grains, which is confirmed to have a very bad effect on the cavity performance. The annealing is a necessary procedure in the vapor diffusion method corresponding to our experimental results.

Author Contributions: Conceptualization, G.W., S.Q., S.H., X.Y. and K.Z.; methodology, G.W., L.L., M.R., J.H., F.W. and F.J.; software, G.W.; formal analysis, G.W. and S.Q.; investigation, G.W.; writing—original draft preparation, G.W.; writing—review and editing, S.Q., J.H. and F.Z.; supervision, S.Q. and S.H. All authors have read and agreed to the published version of the manuscript.

Institutional Review Board Statement: Not applicable.

Informed Consent Statement: Not applicable.

Data Availability Statement: The data presented in this study are available on request from the corresponding author.

Conflicts of Interest: The authors declare no conflict of interest.

References

1. Valente-Feliciano, A.-M. Superconducting RF materials other than bulk niobium: A review. *Supercond. Sci. Technol.* **2016**, *29*, 113002. [CrossRef]
2. Hillenbrand, B. The Preparation of Superconducting Nb_3Sn Surfaces for RF Applications. In Proceedings of the SRF Workshop, Karlsruhe, Germany, 2–4 July 1980; pp. 41–52.

3. Peiniger, M.; Hein, M.; Klein, N.; Mueller, G.; Piel, H.; Thuenus, P. Work on Nb$_3$Sn Cavities at Wuppertal. In Proceedings of the 3th Workshop on RF Superconductivity, Argonne, IL, USA, 14–17 September 1987; pp. 502–532. Available online: https://accelconf.web.cern.ch/accelconf/srf87/papers/srf87e04.pdf (accessed on 16 October 2020).
4. Müller, G.; Kneisel, P.; Mansen, D. Nb$_3$Sn layers on high-purity Nb cavities with very high quality factors and accelerating gradients. In Proceedings of the 5th European Particle Accelerator Conference, Sitges, Spain, 10–14 June 1996; Available online: https://accelconf.web.cern.ch/e96/PAPERS/WEPL/WEP002L.PDF (accessed on 6 November 2019).
5. Posen, S.; Liepe, M. Nb$_3$Sn–Present Status and Potential as an Alternative SRF Material. In Proceedings of the 27th LINAC, Geneva, Switzerland, 31 August–5 September 2014; Available online: https://accelconf.web.cern.ch/LINAC2014/papers/tuioc03.pdf (accessed on 15 October 2020).
6. Porter, R.; Arias, T.; Cueva, P.; Sitaraman, M.N.; Hall, D.L.; Liepe, M.; Maniscalco, J.T. Next Generation Nb$_3$Sn Cavities for Linear Accelerators. In Proceedings of the 29th LINAC, Beijing, China, 16–21 September 2018; pp. 462–464. [CrossRef]
7. Pudasaini, U.; Eremeev, G.; Reece, C.; Kelley, M.J.; Parajuli, I.P. Recent Results from Nb3Sn Coated Single-cell Cavities Combined with Sample Studies at Jefferson Lab. In Proceedings of the 10th IPAC'19, Melbourne, Australia, 19–24 May 2019; pp. 3066–3069. [CrossRef]
8. Posen, S.; Lee, J.; Seidman, D.N.; Romanenko, A.; Tennis, B.; Melnychuk, O.S.; Sergatskov, D.A. Advances in Nb$_3$Sn super-conducting radiofrequency cavities towards first practical accelerator applications. *Supercond. Sci. Technol.* **2021**, *34*, 025007. [CrossRef]
9. Posen, S.; Hall, D. Nb$_3$Sn superconducting radiofrequency cavities: Fabrication, results, properties, and prospects. *Supercond. Sci. Technol.* **2017**, *30*, 033004. [CrossRef]
10. Posen, S.; Gonnella, D.; Liepe, M. Recent Progress in Nb$_3$Sn SRF Cavity Development at Cornell. In Proceedings of the 5th IPAC, Dresden, Germany, 15–20 June 2014. [CrossRef]
11. Eremeev, G. Results from the First Single-cell Nb$_3$Sn Cavity Coatings at JLAB. In Proceedings of the 6th IPAC'15, Richmond, VA, USA, 3–8 May 2015; pp. 3509–3511. [CrossRef]
12. Eremeev, G.; Pudasaini, P. Development of Nb$_3$Sn Multicell Cavity Coatings. In Proceedings of the IPAC'19, Melbourne, Australia, 19–24 May 2019; pp. 3070–3073. [CrossRef]
13. Takahashi, K.; Kako, E.; Umemori, K.; Saka, H.; Konomi, T. First Nb3Sn Coating and Cavity Performance Result at KEK. In Proceedings of the SRF'21, East Lansing, MI, USA, 27 June–2 July 2021; Available online: https://indico.frib.msu.edu/event/38/attachments/158/1149/SUPCAV009_poster.pdf (accessed on 17 December 2020).
14. Dong, C.; Lin, Z.; Sha, P.; Liu, B.; Ye, L.; He, X. Preliminary Research of Niobium Cavity Coating with Nb$_3$Sn Film at IHEP. *Phys. C Supercond. Its Appl.* **2022**, *600*, 1354107. [CrossRef]
15. Yang, Z.; Huang, S.; He, Y.; Lu, X.; Guo, H.; Li, C.; Niu, X.; Xiong, P.; Song, Y.; Wu, A.; et al. Low-Temperature Baking Effect of the Radio-Frequency Nb$_3$Sn Thin Film Superconducting Cavity. *Chin. Phys. Lett.* **2021**, *38*, 092901. [CrossRef]
16. Lee, J.; Mao, Z.; He, K.; Sung, Z.H.; Spina, T.; Baik, S.-I.; Hall, D.L.; Liepe, M.; Seidman, D.N.; Posen, S. Grain-boundary structure and segregation in Nb$_3$Sn coatings on Nb for high-performance superconducting radiofrequency cavity applications. *Acta Mater.* **2020**, *188*, 155–165. [CrossRef]
17. Carlson, J.; Pack, A.; Transtrum, M.K.; Lee, J.; Seidman, D.N.; Liarte, D.B.; Sitaraman, N.S.; Senanian, A.; Kelley, M.M.; Sethna, J.P.; et al. Analysis of magnetic vortex dissipation in Sn-segregated boundaries in Nb$_3$Sn superconducting RF cavities. *Phys. Rev. B* **2021**, *103*, 024516. [CrossRef]
18. Wang, Q.-Y.; Xue, C.; Dong, C.; Zhou, Y.-H. Effects of defects and surface roughness on the vortex penetration and vortex dynamics in superconductor–insulator–superconductor multilayer structures exposed to RF magnetic fields: Numerical simulations within TDGL theory. *Supercond. Sci. Technol.* **2022**, *35*, 045004. [CrossRef]
19. Porter, R.; Furuta, F.; Hall, D.L.; Liepe, M.; Maniscalco, J.T. Effectiveness of Chemical Treatments for Reducing the Surface Roughness of Nb$_3$Sn. In Proceedings of the IPAC'17, Copenhagen, Denmark, 14–19 May 2017; Available online: https://accelconf.web.cern.ch/ipac2017/papers/mopva124.pdf (accessed on 14 October 2022).
20. Pudasaini, U.; Eremeev, G.; Reece, C.; Tuggle, J.; Kelley, M.G. Post-processing of Nb$_3$Sn Coated Niobium. In Proceedings of the IPAC'17, Copenhagen, Denmark, 14–19 May 2017; Available online: https://accelconf.web.cern.ch/ipac2017/papers/mopva144.pdf (accessed on 30 November 2021).
21. Pudasaini, U.; Eremeev, G.; Reece, C.; Tian, H.; Kelley, M.G. Electrochemical Finishing Treatment of Nb$_3$Sn Diffusion-coated Niobium. In Proceedings of the SRF'17, Lanzhou, China, 17–21 July 2017. [CrossRef]
22. Mucklejohn, S.; O'Brien, N. The vapour pressure of tin (II) chloride and the standard molar Gibbs free energy change for formation of $SnCl_2$(g) from Sn(g) and Cl_2(g). *J. Chem. Thermodyn.* **1987**, *19*, 1079–1085. [CrossRef]
23. Meurant, G. *Advances in Chemical Engineering*, 2nd ed.; Elsevier Science: Amsterdam, The Netherlands, 1958.
24. Loeb, L. *The Kinetic Theory of Gases*, Dover phoenix, ed.; Dover Publications: Mineola, NY, USA, 2004; ISBN 978-0486495729.
25. Ridgway, R. Simulating Nb3Sn Coating Process inside SRF Cavities. Available online: https://indico.fnal.gov/event/14933/contributions/28540/attachments/17987/22615/Simulating_Nb3Sn_Coating_Process_Inside_SRF_Cavities_-_Robert_Ridgway.pdf (accessed on 18 November 2021).
26. Pudasaini, U.; Eremeev, G.V.; Reece, C.E.; Tuggle, J.; Kelley, M.J. Initial growth of tin on niobium for vapor diffusion coating of Nb$_3$Sn. *Supercond. Sci. Technol.* **2019**, *32*, 045008. [CrossRef]

27. Standard Test Methods for Determining Average Grain Size. Available online: https://mse.engin.umich.edu/internal/lab-modules/microscopy-and-microstructure-analysis/grain-size-determination (accessed on 29 October 2021).
28. Posen, S.; Hoffstaetter, G.; Liepe, M.; Xie, Y. Resent Developments in the Cornell Nb_3Sn Initiative. In Proceedings of the IPAC'12, New Orleans, LA, USA, 12–17 June 2012; Available online: https://accelconf.web.cern.ch/IPAC2012/papers/weppc078.pdf (accessed on 28 October 2019).
29. El-Agez, T.; Taya, S. Design of a spectroscopic ellipsometer by synchronous rotation of the polarizer and analyzer in opposite directions. *Microw. Opt. Technol. Lett.* **2014**, *56*, 2822–2826. [CrossRef]